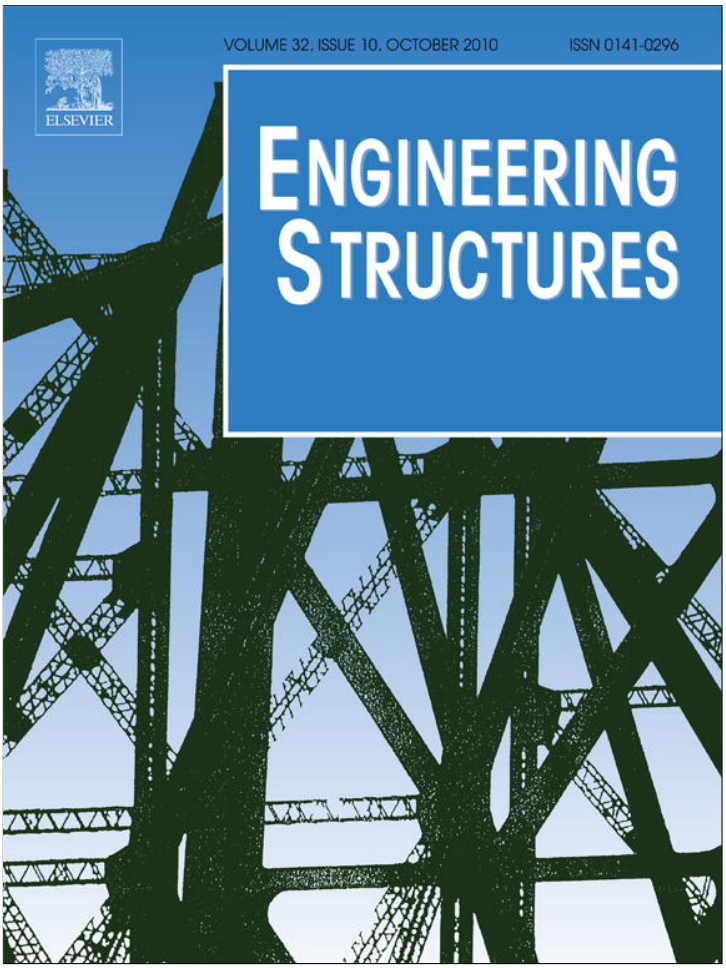

Engineering Structures 32 (2010) 2995–3010

Contents lists available at ScienceDirect

Engineering Structures

journal homepage: www.elsevier.com/locate/engstruct

Analytical study on seismic retrofitting of reinforced concrete buildings using steel braces with shear link

Cengizhan Durucan, Murat Dicleli *

Department of Engineering Sciences, METU, 06531, Turkey

ARTICLE INFO

Article history:
Received 25 November 2009
Received in revised form
28 May 2010
Accepted 29 May 2010
Available online 29 June 2010

Keywords:
Seismic retrofitting
Reinforced concrete
Building
Shear link
Performance based design

ABSTRACT

This paper is focused on a proposed seismic retrofitting system (PRS) configured to upgrade the performance of seismically vulnerable reinforced concrete (RC) buildings. The PRS is composed of a rectangular steel housing frame with chevron braces and a yielding shear link connected between the braces and the frame. The retrofitting system is installed within the bays of an RC building frame to enhance the stiffness, strength and ductility of the structure. The PRS and a conventional retrofitting system using squat infill shear panels (SISPs) are used in an existing school and an office building. Nonlinear time history analyses of the buildings in the original and retrofitted conditions are conducted for three different seismic performance levels (PLs) to assess the efficiency of the PRS. The analyses results revealed that the building retrofitted with the PRS has a more stable lateral force–deformation behavior with enhanced energy dissipation capability than that of the one retrofitted with SISPs. For immediate occupancy PL, the maximum inter-storey drift of the building retrofitted with the PRS is comparable to that of the one retrofitted with SISPs. But for life safety and collapse prevention PLs, the maximum inter-storey drift of the building retrofitted with the PRS is considerably smaller than that of the one retrofitted with SISPs. Furthermore, compared with the building retrofitted with SISPs, the building retrofitted with the PRS experiences significantly less damage due to the more ductile behavior of the system at the life safety and collapse prevention PLs.

1. Introduction

In many areas around the world, reinforced concrete (RC) buildings designed using codes that are now known to provide inadequate safety under seismic forces are potential hazards. In such areas, the number of RC buildings built prior to 1980 outnumbers those that are built according to the newer codes. Therefore, these structurally deficient buildings should be retrofitted to withstand earthquake forces in compliance with modern design codes.

There are many well known seismic retrofitting methods for RC structures. These methods can be classified into two groups as: (i) conventional methods, based on improving the strength, stiffness and ductility of the structure, and (ii) innovative response modification methods (RMMs) aimed at alleviating the effect of seismic forces on structures. Conventional methods include techniques such as adding RC infill walls to the structural system and jacketing of RC columns [1,2]. The main advantage of these methods is that they can be easily designed and applied using conventional construction techniques. However, conventional methods have some technical and practical disadvantages. Strengthening the RC columns by jacketing and/or adding RC infill walls results in an increase in the weight of the structure that produces larger earthquake forces. Furthermore, these methods require heavy demolition and construction work [3]. Innovative RMMs on the other hand include techniques such as installing seismic isolation devices or dampers in the building. These devices are intended to modify the seismic response of the building so as to alleviate the effect of the seismic forces. Several retrofitting applications using RMMs exist in many parts of the world [4,5]. Retrofitting techniques based on RMMs have significant advantages with respect to conventional seismic retrofitting methods. RMMs are very effective in reducing the detrimental effects of earthquakes on buildings. These methods usually do not require heavy demolition or construction work when used for seismic retrofitting. Nevertheless, such methods are generally costly to implement [6]. This makes them unsuitable for ordinary buildings. Most applications of RMMs are therefore found in important government or historical buildings, museums or hospitals [4].

In light of the above discussion, it is clear that in addition to the advantages of each retrofitting method, there are numerous disadvantages. Consequently, a seismic retrofitting system that combines the advantages of both conventional and modern retrofitting techniques is required. Accordingly, this research study is focused on a proposed steel link-brace retrofitting system configured to upgrade the performance of seismically vulnerable RC buildings by combining the advantages and eliminating most

* Corresponding author. Tel.: +90 312 210 4451; fax: +90 312 210 4462.
E-mail address: mdicleli@metu.edu.tr (M. Dicleli).

0141-0296/$ – see front matter © 2010 Elsevier Ltd. All rights reserved.
doi:10.1016/j.engstruct.2010.05.019

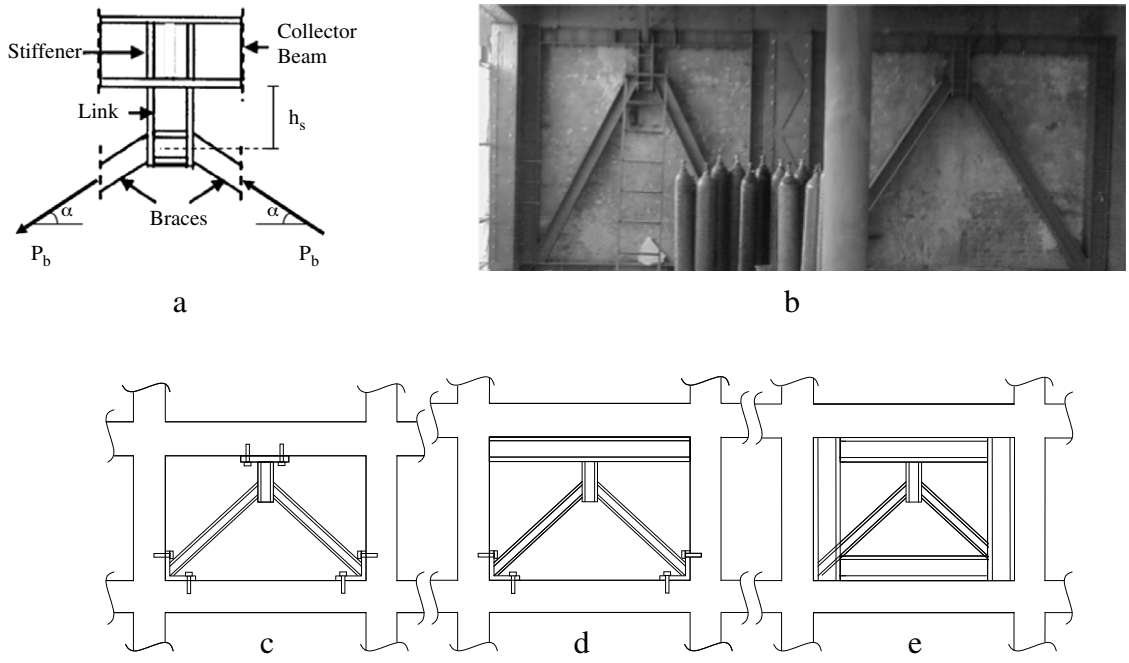

Fig. 1. (a) Proposed seismic retrofitting system [8]. (b) Recent application of the proposed retrofitting system to an office building. (c) Configuration 1 of the proposed retrofitting system. (d) Configuration 2 of the proposed retrofitting system. (e) Configuration 3 of the proposed retrofitting system.

of the disadvantages of conventional and modern response modification retrofitting techniques for RC buildings.

2. Research outline

This research study is aimed at studying the efficiency of the proposed retrofitting system (PRS). The efficiency of the PRS is studied using a two-stories school building and a six-stories office building. These buildings are retrofitted using the PRS and a conventional system composed of squat infill shear panels (SISPs). The performance of the buildings retrofitted with the PRS is then assessed in relation to those of the original buildings and the buildings retrofitted with SISPs. For this purpose, first, three possible configurations of the PRS suitable for RC buildings are outlined. Then, 2-D and 3-D finite element analyses of a sample two-stories RC frame with the three different PRS configurations are conducted. From the analyses results, the most efficient retrofitting configuration is selected and used throughout this study. Subsequently, site specific response spectra (SSRS) are obtained for retrofitting the design of the buildings used in this study and to obtain response spectrum (RS) compatible ground motions for the seismic performance assessment of the buildings. Next, a performance based retrofitting design procedure that involves RS and nonlinear static pushover (NLSP) analyses is developed and used for the design of the buildings. Following this, the seismic performance of the buildings retrofitted with the PRS is assessed in relation to those of the original buildings and the buildings retrofitted with the SISP via three types of analyses. First, RS analyses are conducted to determine the load pattern along the height of the buildings for NLSP analyses. NLSP analyses are then conducted to determine the drift limits of the buildings based on FEMA 356 [7] rotation limits and to observe the behavior of the structures under monotonic lateral load. Next, nonlinear time history (NLTH) analyses are conducted to obtain the maximum drifts, member rotations and the deformed shapes of the buildings at the instant of maximum interstorey drifts at three different seismic performance levels (PLs). The maximum interstorey and roof drifts are then compared with the drift limits of the buildings at various PLs to assess the seismic performance of the buildings retrofitted with the PRS in relation to those of the original buildings and the buildings retrofitted with SISP. Damage analyses are also conducted as an additional measure of the seismic performance of the buildings.

3. Proposed seismic retrofitting system

Steel braces are often used for seismic retrofitting of RC buildings. However, when subjected to strong ground motions, the buckling of the braces results in loss of lateral stiffness and strength of the structural system [8]. Thus, seismic retrofitting of RC buildings with braces that may potentially buckle does not seem to be a feasible retrofitting solution. Hence, this research study is focused on a PRS that is capable of dissipating the earthquake input energy without buckling of the braces. The PRS is composed of chevron braces and an energy dissipating shear link connected between the braces and the beam. Fig. 1(a) and (b) show a sketch and a photograph from a recent application of the PRS by the authors to an office building. Similar design or retrofitting schemes found in the literature use special (or unconventional) energy dissipation devices such as T-ADAS [9] (Triangular-Added Damping and Stiffness) yielding under flexural effects. In the PRS however, the shear link is designed to yield in shear before the compression brace buckles to prevent lateral strength and stiffness degradation associated with brace buckling. In the shear link, the shear force created by the braces is constant along its length. This allows for the development of large plastic deformations without excessive local strains that normally occur in flexural yielding [9]. Consequently, shear yielding provides more effective energy dissipation than that of flexural yielding [10] and, hence, it is adopted for the design of the link in the PRS. The link may be built either using a compact steel HP, a European HE or a web-stiffened W section. For the retrofitting of RC buildings, the PRS is inserted into the bays of the RC frames to improve the stiffness, strength and energy dissipation capacity of the building as shown in Fig. 1(c)–(e). The PRS can be applied in various configurations where (i) the link and the braces

Table 1
2-D finite element analyses results.

Configuration	Stiffness (kN/m)	Base shear (kN)	Displacement (mm)	Axial stress (MPa)		Shear stress (MPa)	
				Column	Beam	Column	Beam
1	32,500	450	13.8	9.4	16.2	0.9	2
2	40,090	450	11.4	8.1	5.9	0.6	1.9
3	50,609	450	8.9	7.7	5.7	1	2.2
4	3,125	450	144	61.8	61.8	5.4	4.5

are directly connected to the RC members via steel plates, bolts and epoxy grouting (Fig. 1(c) - Configuration (1), (ii) the link is connected to a collector steel beam attached to the concrete beam and the rest of the members are connected to the RC members via steel plates (Fig. 1(d) - Configuration (2) or (iii) the link and the braces are housed in a rectangular steel frame (housing frame) where the steel frame is connected to the RC members by bolts and epoxy grouting (Fig. 1(e) - Configuration (3).

Similar systems have also been proposed by other researchers [11,12]. However, the configurations of the proposed systems in application to RC frames have not been studied and verified. In most cases, the link-brace system was directly applied as a retrofitting solution. In addition, these research studies considered only hypothetical cases with arbitrary retrofitting system configurations that are not based on actual designs. Thus, the performance assessment of the proposed systems may not be realistic. Furthermore, a comparison of the performance of the link-brace system with those of conventional retrofitting methods such as SISPs does not exist in the literature. This study, however, addresses all the issues stated above and provides a performance based seismic retrofitting design methodology for the PRS.

4. Configuration selection through finite element analyses

In this section, finite element modeling and analyses results of a sample two-stories, one-bay RC frame retrofitted using the three configurations introduced above are presented. From the analyses results, the most structurally efficient configuration of the PRS is selected and used throughout this study. The RC frame used in the analyses is extracted from one of the buildings used in this study. The frame is shown in Fig. 2(a). The dimensions of the rectangular columns on the left and right sides of the frame are respectively 0.3 m × 0.6 m and 0.4 m × 0.25 m at the first-storey level and 0.25 m × 0.40 m and 0.40 m × 0.25 m at the second-storey level. The beams at both storey levels have cross sections of 0.25 m × 0.5 m (width × depth). The retrofitting system (link, braces and housing frame) of the sample RC frame is composed of steel HE200M, HE120M and HE220B sections within the first storey and HE180M, HE100M and HE220B sections within the second storey.

The finite element models of the RC frame with various retrofitting configurations are built in two different levels of complexity. The first set of models are 2-D while the second set are 3-D solid models. The 2-D models are built to observe the global distribution of flexural and shear stresses within the RC members of the frame and to assess the stiffness and strength of the RC frame on the verge of yielding of the shear link for the three retrofitting configurations. The more complicated 3-D solid models are used to observe the stress distributions and concentrations within the critical regions of the RC frame around the link and at the corners where the braces are connected to the frame.

4.1. Two dimensional finite element modeling

The 2-D finite element models of the RC frame were built using the nonlinear finite element based software ANSYS [13] as shown in Fig. 2(b)–(d) for the three retrofitting configurations tested. Two different beam elements were used in the finite element modeling of the frame. The RC frame members as well as the shear link and steel frame members of the PRS were modeled using the BEAM189 element in ANSYS [13]. The rigid joints of the RC frame were also modeled using BEAM189 with a large modulus of elasticity. In the case of the steel braces of the retrofitting system, the BEAM44 element is used. BEAM189 is an element suitable for analyzing slender to moderately stubby/thick beam structures. It is based on Timoshenko beam theory. Shear deformation effects are included. This element is well suited for linear, large rotation, and/or large strain nonlinear applications. BEAM44 is a uniaxial element with tension, compression, torsion, and bending capabilities. This element permits the end nodes to have moment releases and be offset from the centroidal axis of the beam. Thus, it is suited for brace modeling.

4.2. Three dimensional solid finite element modeling

The 3-D partial solid models of the critical regions of the RC frame around the link and at the corners where the braces are connected were built to more precisely evaluate the stress concentrations at these locations. The models were built such that the behavior of the overall frame is simulated correctly. This required the structural analyses of the 2-D model of the frame under lateral load before the 3-D partial models could be built. For the region around the link, a local T-shaped section of the frame is modeled in between the inflection points along the beam to investigate the stress distribution within that region as shown in Fig. 2(a) by thick solid lines. For the region around the corner where the brace is connected, a 90° rotated T-shaped section of the frame in between the inflection points along the column (for the vertical member) and along the beam (for the horizontal member) is modeled to investigate the stress distribution within that region as shown in Fig. 2(a) by thick solid lines. The solid models of the critical parts of the frame are built using the program ANSYS [13] as shown in Fig. 2(e) and (f) for the cases with and without a steel housing frame. An automatic mesh generation technique is used for the meshing of the linear elastic solid elements.

4.3. Analyses results

For the 2-D analyses a single lateral load pattern is applied on all the frames. The magnitude and distribution of the lateral load is taken as the average of the loads required to yield the shear link in Configurations 1 and 2. Consequently, the base shear is identical for all the three frames considered. This enabled a fair comparison of the magnitudes of the stresses in the RC members of the frame retrofitted with three different configurations.

The results obtained from the 2-D finite element analyses are comparatively given in Table 1 and Fig. 2(b)–(d). Configuration 4 given in Table 1 is the bare RC frame without the retrofitting system. As observed from Table 1, the retrofitting system with the additional steel frame housing the link and the braces (Configuration 3) produces a structural system with a much higher elastic stiffness compared to Configurations 1 and 2. Consequently, it is expected that the lateral drift of the frame will be smaller when retrofitting Configuration 3 is used. This, in turn, may result in less

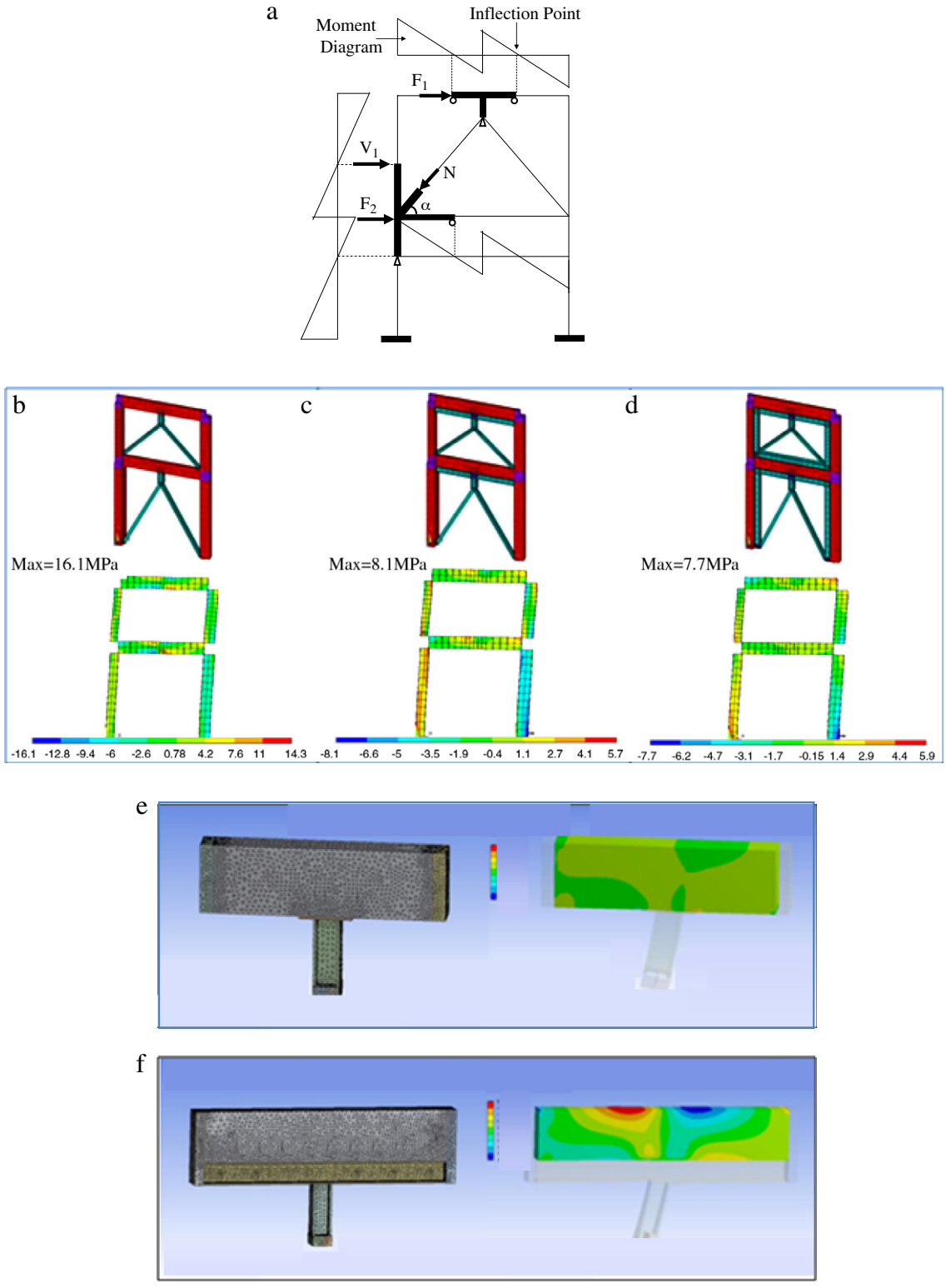

Fig. 2. (a) RC frame used in the 2-D finite element analyses as well as forces and moment diagrams used in the construction of 3-D solid models, (b) 2-D finite element models and axial stresses on RC members; Configuration 1, (c) Configuration 2, (d) Configuration 3, (e) 3-D partial finite element models and axial stresses on RC members; link joint of Configuration 1, (f) link joint of Configuration 3.

damage to the nonstructural and RC structural components of the building during a potential earthquake. Moreover, the presence of the housing steel frame members in Configuration 3 increased the base shear capacity of the building by around 30% (until yielding of the link takes place) compared to Configurations 1 and 2. This means that the building retrofitted with Configuration 3 may remain within the elastic range at higher seismic loads. Configuration 3 is also useful for providing additional vertical support to the RC frame to resist the gravity loads against any potential collapse situation during or after a damaging earthquake. Table 1 also shows the maximum axial (mainly due to bending moment and axial load exerted by the braces) and shear stresses

Table 2
3-D finite element analyses results for the critical joints.

Configuration	Axial stress (MPa)		
	Column (upper)	Column (lower)	Beam
	Upper link joint		
1	N.A	N.A	83
3	N.A	N.A	5.5
	Lower left joint		
1	25	34	20
3	11	7	9.5

within the RC members of the retrofitted frame. For all the cases considered the shear stresses are small. The axial stresses are larger for Configuration 1 and comparable for Configurations 2 and 3. The stresses are more intense around the link, at the joints and at support locations as observed from Fig. 2(b)–(d). The RC members of the bare frame (Configuration 4) have very large concrete axial and shear stresses when it is subjected to the same lateral load as the other retrofitted frames. This clearly shows the benefits of using the proposed retrofitting system even within the elastic range (before the link yields).

The results obtained from 3-D finite element analyses are comparatively evaluated for two configurations (1 and 3) of the proposed seismic retrofitting system. These results are presented in Table 2 for the upper link joint and the lower left joint of the sample frame for the two analyses cases considered. The distributions of the axial stresses are shown in Fig. 2(e) and (f) for the link joint respectively for Configurations 1 and 3. The results for the lower left joint are similar. The analyses results revealed that high axial stress concentrations around the connections of the link and the braces to the RC frame members occur in the case of Configuration 1. This is indicative of local damage to the concrete members. Such local damage may be amplified under cyclic loading resulting in loosening of the connections of the steel members to the RC members of the frame. In the case of Configuration 3 however, the presence of the steel housing frame results in a more even distribution of forces transferred from the link and braces to the RC members of the frame. This results in much lower stresses in the RC members as noted from the 5.5 MPa and 10 MPa stresses in Table 2.

The findings from the analyses of more refined 3-D solid models are in good agreement with those from the analyses of the 2-D models. Consequently, it is expected that Configuration 3 will offer a better seismic retrofitting solution for RC buildings. Accordingly, Configuration 3 is selected for the retrofitting of the buildings used in this study.

5. Description of the buildings used in this study

Two existing buildings are selected to study the structural performance with the PRS. The buildings have some common properties. These properties are; nearly symmetrical floor plans, a moment resisting RC frame system (i.e. no shear walls) and poorly detailed RC structural members. Furthermore, both buildings are located in areas with a high risk of seismic activity. Both buildings have major deficiencies according to the current Turkish seismic design code [14]. These deficiencies are; insufficient confinement of the columns in the plastic hinging region, inadequate member sizes according to the code, (200 × 350 mm is the minimum allowed member cross section area), lack of capacity protected design that leads to shear failure in some members, the use of plain bars in the construction where the code requires deformed bars, inadequate concrete compressive strength and lack of shear walls in the structural system of both buildings.

The first building is a two-storey school building. A photograph of the building and a typical floor plan are shown in Fig. 3(a) and (b). The school was built in 1987 in compliance with the 1975 Turkish Seismic Design Code [15]. Therefore, the seismic capacity of the building is not sufficient according to the current 2007 edition of the same code [14]. It is noteworthy that the Turkish seismic design code for buildings is very similar to the International Building Code [16]. Site soil type is classified as type C per Turkish Seismic Design Code [14] or International Building Code [14]. The heights of the first and second stories are 3.2 m. The slab thickness is 0.20 m in the first and 0.15 m in the second storey. The first and second-storey structural member sizes are identical. The dimensions of most of the rectangular columns are 0.3 × 0.5 m while the remaining columns near the wider bays have cross sections larger than 0.3 × 0.5 m and up to 0.55 × 0.50 m. All the beams supporting the large 7.2 × 7.2 m slabs are 0.3–0.4 m wide and 0.7 m deep, while the remaining beams are 0.3 m wide and 0.50 m deep. The RC frame bays of the building are filled with brick masonry infill (BMI) walls. The materials considered in the modeling and retrofitting design are a low strength concrete class C16 (f_c = 16 MPa and E_c = 18,800 MPa) and the plain reinforcing steel bars of class St.220 (f_{sy} = 220 MPa and E_s = 200,000 MPa) according to Turkish standards. The second building is a six-storey RC office building. A photograph of the building and a typical floor plan are shown in Fig. 3(c) and (d). The building was built in 1954. Therefore, the seismic capacity of the building is not sufficient according to the current Turkish seismic design code [14]. The soil characteristic of the site is classified as group D. The height of the first storey (basement) is 2.9 m while that of the second storey is 3.85 m (above the entrance floor). The heights of the remaining stories are 2.75 m. The slab thickness is 0.10 m in all the stories. The beam sizes (0.1 m wide and 0.50 m deep) in all the stories are generally identical and the column sizes gradually decrease from 0.5 × 0.5 m at the lower-storey levels to 0.2 × 0.2 m at the upper-storey levels. Most of the RC frame bays are filled with timber window frames and a limited number of them are filled with thin gypsum walls with negligible structural resistance. The materials considered in the modeling and retrofitting design are a low strength concrete class C13 (f_c = 13 MPa and E_c = 16,900 MPa.) and the plain reinforcing steel of class St.220 (f_{sy} = 220 MPa and E_s = 200,000 MPa).

For the two buildings, the RC members that may fail in shear prior to the formation of flexural plastic hinges at the member ends are determined. For the school building, it is found that none of the members fail in shear prior to the formation of flexural plastic hinges. However, for the office buildings, It is found that a few columns lack adequate shear capacity to allow for flexural plastic hinge formation. To prevent such a poor seismic performance, these members are retrofitted using four steel angles attached by bolts and epoxy grouting at column corners and horizontal and diagonal braces connected between the steel angles to upgrade the shear capacity while keeping the flexural capacity at the same level as shown in Fig. 3(e) (the steel angles used are terminated at a distance of 50 mm from the member ends to avoid flexural strengthening). Following this local retrofitting, none of the members will fail in shear prior to the formation of flexural plastic hinges at the member ends. Moreover, in the case of the office building the seismic retrofitting of the foundation was not required but for the case of the school building a limited strengthening of the foundations was performed.

6. Site specific response spectra

In this study, SSRS are mainly required for conducting RS analyses as part of the iterative seismic retrofitting design procedure, for determining the lateral load pattern along the height of the building for NLSP analyses and for obtaining site specific ground motions for NLTH analyses conducted for the

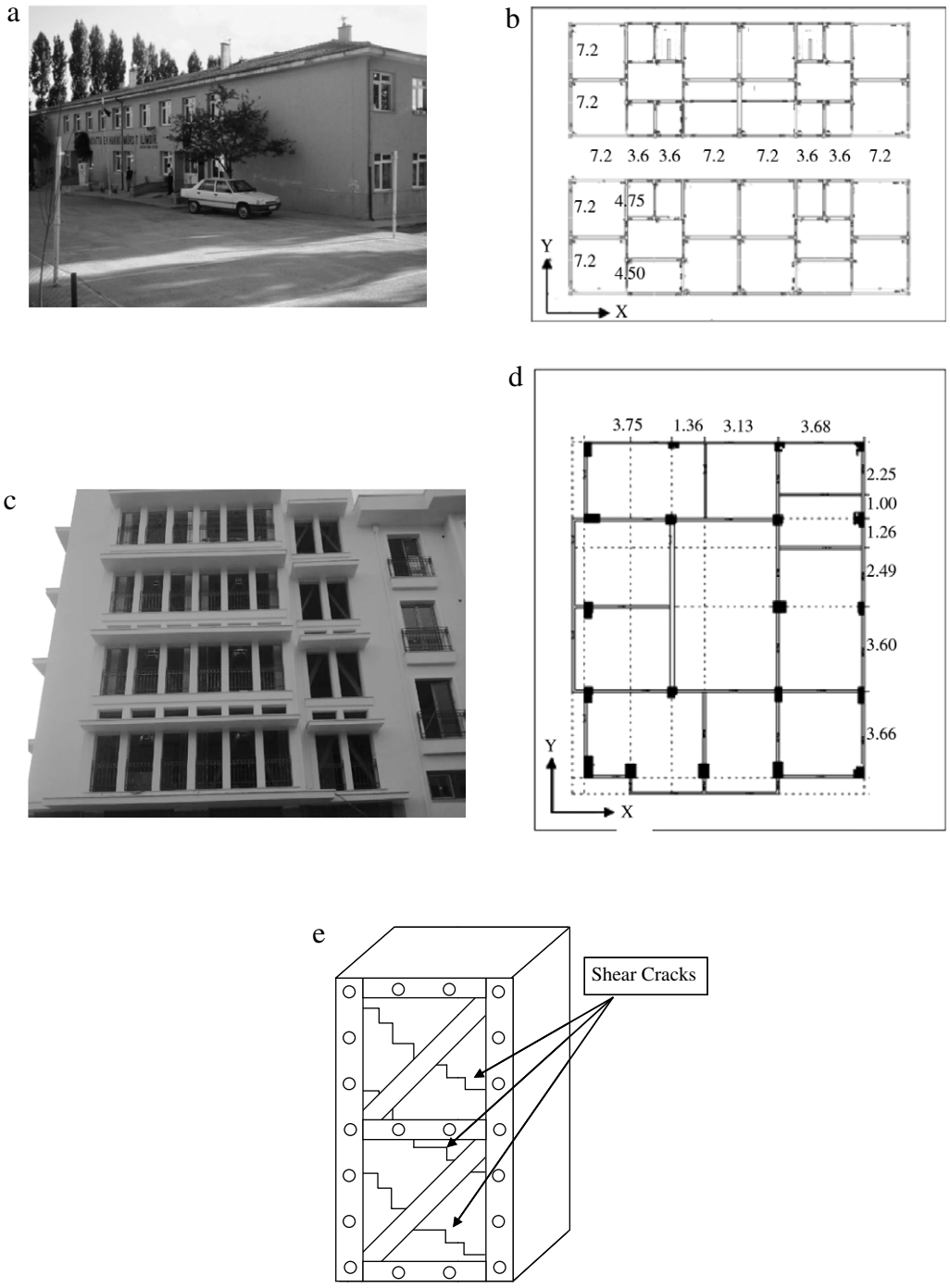

Fig. 3. (a) School building. (b) Floor plans of the school building. (c) Office building. (d) Typical floor plan of the office building (dimensions are in meters). (e) Column retrofitting scheme.

seismic performance assessment of the buildings. The procedure for constructing the SSRS for the buildings under consideration is taken from the Turkish Republic Ministry of Transportation Railways, Harbors and Airports Construction General Directorate Design Code [17]. The procedure requires the site soil type and location coordinates of the buildings to obtain the necessary parameters for constructing the SSRS. SRSS are obtained for three different earthquake levels with different probabilities of being exceeded (50% in 50 years, 10% in 50 years and 2% in 50 years) for the performance based seismic retrofitting design and analyses of the buildings under consideration. Fig. 4(a) and (b) show the plots of the SRSS for the three earthquake levels used in the retrofitting design and seismic performance assessment of the school and office buildings respectively.

7. Response spectra compatible ground motions

Based on the requirements of the International Building Code [16] SSRS compatible ground motions are selected as follows. First, seven earthquake ground motions whose response spectra are compatible with the SSRS are selected from the PEER (Pacific Earthquake Engineering Research) strong motion database. Details of the selected ground motions are given in Table 3. Each one of these ground motions were first scaled to PGAs of the SSRS for the

Table 3
Selected earthquakes and their properties.

Earthquake	Station/component	Soil type	Ap (g)	Vp (cm/s)	Ap/Vp (1/s)	ID no.
Whittier Narrows 1987	90079 Downey - Birchdale/ 180	D	0.299	37.8	7.8	1
Imperial Valley 1979	6605 Delta/ 262	D	0.238	26	9.0	2
Coalinga 1983	46314 Cantua Creek School/ 270	D	0.227	23.6	9.4	3
Loma Pri eta 1989	1656 Hollister Diff. Array/ 255	D	0.279	35.6	7.7	4
Imperial Valley 1979	2316, BONDS CORNER, 230	D	0.113	11.1	10.0	5
Imperial Valley 1940	117 El Centro Array #9/ 270	D	0.215	30.2	7.0	6
Westmorland 1981	5169 Westmorland Fire Sta/90	D	0.368	48.7	7.4	7

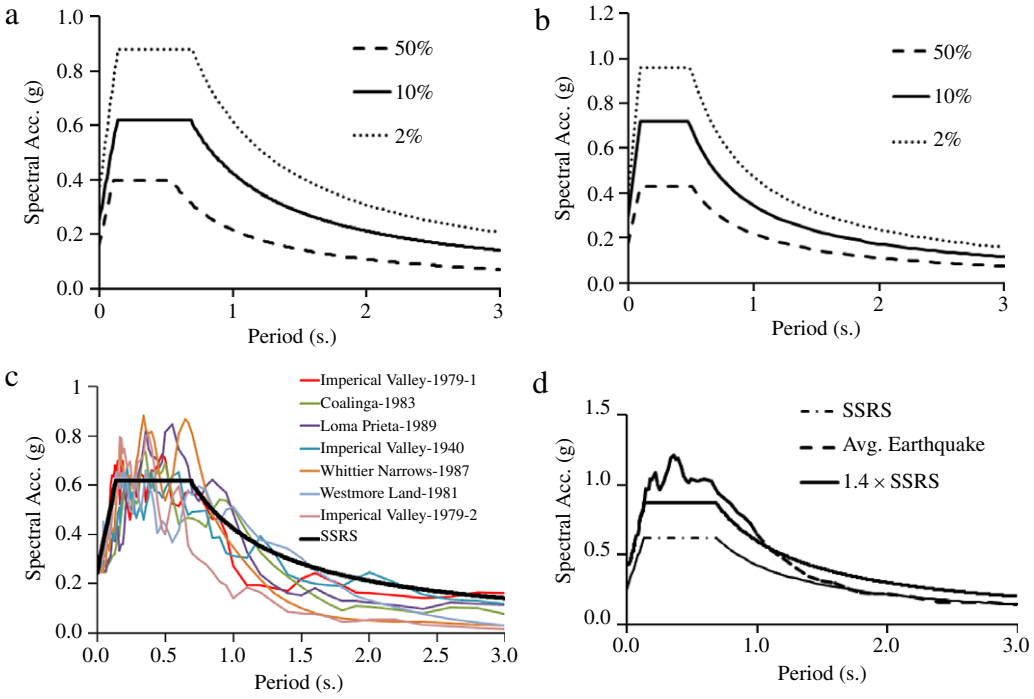

Fig. 4. (a) SSRS for school building. (b) SSRS for office building. (c) Design spectrum and acceleration spectra of the ground motions scaled to the PGA of the design spectrum. (d) Comparison of the average of the scaled earthquake ground motions with the design spectrum and 1.4 × the design spectrum.

three earthquake levels (50% in 50 years, 10% in 50 years and 2% in 50 years). Following this initial scaling procedure, the average value of the already scaled seven SSRS compatible ground motions were rescaled to obtain an average value larger than or equal to 1.4 times the SSRS within a period range of $0.2T$–$1.5T$ where T is the fundamental period of the building ($T = 0.53$ s for the school building and $T = 0.87$ s for the office building). Fig. 4(c) shows the response spectra of the selected earthquakes and the SSRS for the school building for the earthquake level associated with 10% probability of being exceeded in 50 years. Fig. 4(d) shows the comparison of the average of the scaled ground motions with the SSRS and 1.4 × SSRS. Response spectra for the other earthquake levels and the office building are similar. Therefore, the same earthquake accelerograms, but scaled using different factors, were used in the seismic performance assessment of the two buildings.

8. Nonlinear modelling of existing buildings

NLSP and NLTH analyses are conducted to assess the seismic performance of the original and retrofitted buildings used in this research study. For this purpose, nonlinear structural models of the school building and office building are built and analyzed using the program SAP2000 [18]. These structural models are capable of simulating the nonlinear behavior of the structural components. The RC beams and columns as well as the steel components of the PRS are modeled using 3-D beam elements. The BMI walls are modeled using diagonal beam elements with end moment releases while the SISPs are modeled using a combination of rigidly connected two horizontal and one vertical beam elements. The nonlinear behavior of the structural members are simulated by using nonlinear link/hinge (link for NLTH and hinge for NLSP analyses) elements connected at appropriate locations or at the ends of the beam elements. Typical structural modeling configurations used in SAP2000 [18] are shown in Fig. 5(a) for RC columns and beams, 5(b) for BMI walls, 5(c) for the steel components of the PRS and 5(d) for SISPs.

8.1. Modeling of the RC columns and beams for NLTH analyses

The nonlinear behavior of the RC columns and beams of the buildings used in this study are defined in the structural model by using nonlinear flexural link elements at the ends of the beam/column members. Takeda et al.'s [19] (Fig. 5(e)) hysteresis model is the most commonly accepted model for defining the nonlinear behavior of RC members [20] and it is used in the analyses. Takeda et al.'s [19] model uses the monotonic moment curvature (or rotation) relationship of the RC section as a backbone curve. Therefore, an accurate estimation of the moment curvature relationship is important to correctly simulate the nonlinear cyclic behavior of an RC member.

To obtain the moment–curvature relationship of the RC members of the buildings used in this study, computer software

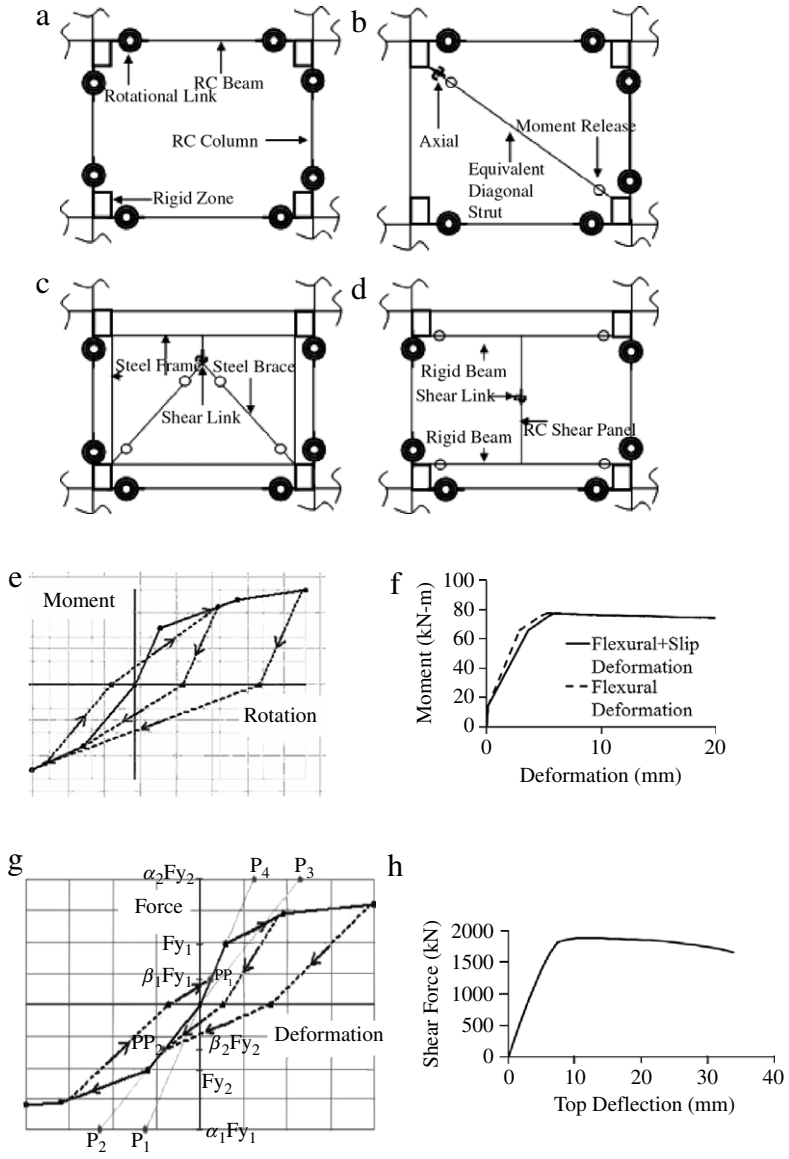

Fig. 5. Nonlinear link elements and other structural elements used in the nonlinear modeling of an example building: (a) RC frame, (b) BMI wall, (c) proposed seismic retrofitting system, (d) squat infill shear panel, (e) Takeda et al.'s hysteretic model, (f) slip effect on moment-deformation graph, (g) pivot hysteretic model, (h) shear force deformation relation of squat infill shear panels.

that was developed by Yalçın and Saatçioğlu [21] was used. The software, referred to as COLA (**Col**umn **A**nalysis), provides sectional moment–curvature analyses and member analyses, including P–Δ effects, buckling and anchorage slip of the reinforcement bars. Including the effect of anchorage slip in the moment curvature relationship becomes especially important for plain bars where slippage is more likely. Therefore, the effect of the anchorage slip is included in the moment curvature relationship of the RC members of the buildings used in this study. Fig. 5(f) show the moment versus lateral displacement relationship of a typical RC member from the school building. In the figure, the analyses results with and without anchorage slip are shown. The different moment–displacement relationships clearly show the importance of including the anchorage slip for more accurate estimation of RC member behavior.

8.2. Modeling of RC squat infill shear panels for NLTH analyses

SISPs were used for the conventional seismic retrofitting of the buildings employed in this research study. SISPs are structural elements where shear behavior is more dominant. Pinching is a common phenomenon in the hysteretic shear force–deformation relationships of SISPs [22,23]. Pinching reduces the area under the hysteresis loop and hence the energy dissipated by SISPs. Consequently, this behavior should be considered in the hysteretic models of the SISPs. In this study, the hysteretic shear force deformation behavior of SISPs was simulated with the pivot hysteresis model [24] (Fig. 5(g)) available in SAP2000 [20]. The model requires the shear force–deformation envelope as well as two additional parameters: the stiffness degradation parameter, α, and the pinching parameter, β, for capturing the stiffness degradation and pinching properties of RC members.

To obtain the shear force–deformation envelope of the SISPs used for conventional retrofitting, the softened truss model of Hsu and Mo [25] is employed in the analyses. The stress–strain curve proposed by Vechio and Collins [26] is used for the softened diagonal concrete struts of the softened truss model. The analyses are conducted following an iterative solution procedure proposed by Mansour et al. [27] A typical shear force deformation envelope obtained from the iterative analysis procedure is shown in Fig. 5(h).

In the literature, there are a limited number of reliable data defining the stiffness degradation parameter, α, and the pinching parameter, β. Lack of analytical tools for defining these parameters forced several researchers to conduct many experimental studies to obtain these parameters [28–32]. A set of test specimens with properties similar to those of the SISPs used in this study were investigated. Then, the necessary parameters for the shear panels employed in this study are obtained as $\alpha = 9.68$, $\beta = 0.41$ by using the average of the experimental test results from these research studies [28–32].

8.3. Modeling of brick masonry infills for NLSP analyses

Modeling the behavior of BMIs is quite complex and the presence of window or door holes makes this task even more difficult. There are some modeling techniques in the literature. The common ground of these techniques is using diagonal struts to model BMIs [33]. In this study, the diagonal strut modeling procedure of FEMA 356 [7] is used to model the BMIs for the NLSP analyses of the school building (Fig. 5(b)). From the NLSP analyses it is found that the BMI walls fail at very small displacements. Comparative NLTH analyses of sample frames with and without BMIs obtained from the school building also show comparable results. Thus, BMI walls are not included in the NLTH analyses of the school building,

8.4. Modeling of proposed steel retrofitting system for NLTH analyses

For NLTH analyses, the hysteretic behavior of the shear link in the PRS is modeled by using the plastic Wen element in SAP2000 [18], which has an elasto-plastic shear force displacement hysteresis. The yield force and displacement of the link are used to define the plastic Wen element. The steel frame members and the braces are modeled using beam elements. The steel beam elements of the steel housing frame are connected to the nodes at the ends of the rigid elements defining the RC joints (Fig. 5(c)).

9. Seismic retrofitting design of the buildings

A performance based approach is used for the seismic retrofitting design of the buildings considered in this study. The performance based design approach is based on matching various probable earthquakes with target PLs. Three target PLs are used for the retrofitting design of the buildings as follows: (i) Immediate Occupancy (IO) PL where no damage is expected for minor levels of earthquake excitations, (ii) Life Safety (LS) PL where low or repairable structural and non-structural damage is expected for moderate earthquake excitations, and (iii) Collapse Prevention (CP) PL where irreparable or hardly repairable structural and non-structural damage but no collapse is expected for major earthquake excitations. In FEMA 356 [7], these target PLs are mainly defined by plastic rotation limits of the RC members. Recent research conducted by Acun and Sucuoğlu revealed that the rotation limits of Eurocode 8 and ASCE/SEI 41(FEMA 356) are suitable for RC building construction in Turkey [34]. These limits are used in the retrofitting design of the buildings to define each PL.

Ground motion levels, which represent the aforementioned minor, moderate and major earthquakes are as follows: (i) minor earthquakes are defined as frequent earthquakes, which have 50%/probability of being exceeded in 50 years (72 years return period), (ii) moderate earthquakes are defined as having a moderate probability of occurrence during the economical life of a structure and have 10% probability of being exceeded in 50 years (475 years return period) and (iii) major earthquakes are defined as less frequent earthquakes which have only 2% probability of being exceeded in 50 years (2475 years return period).

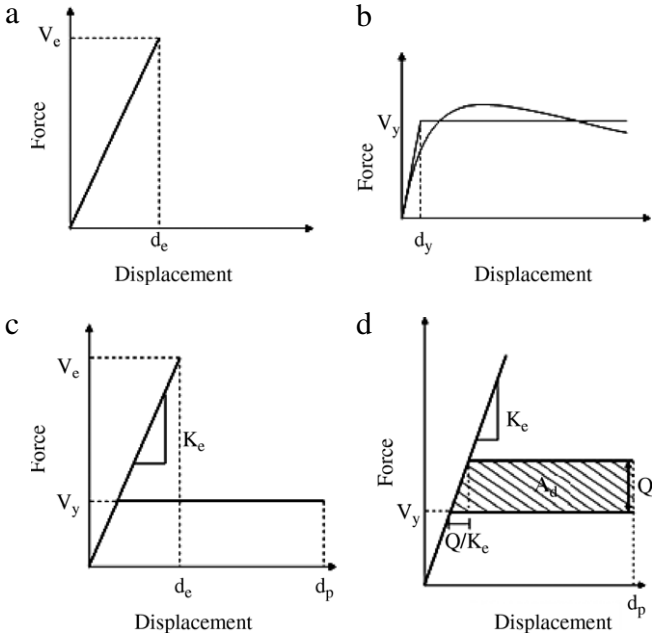

Fig. 6. (a) Linear elastic base shear force vs. roof displacement relationship. (b) Elasto-plastic base shear force vs. roof displacement relationship. (c) Elastic vs. plastic base shear force -roof displacement relationships. (d) Calculation of required strength, Q.

9.1. Retrofitting design procedure

The iterative procedure employed in the seismic retrofitting design of the buildings is outlined in this section. The procedure involves both RS and NLSP analyses. The earthquake effects on the buildings are represented by SSRS obtained for each one of the aforementioned PLs in the retrofitting design. The buildings should achieve the performance criteria defined earlier by limiting the RC member rotations by the rotation limits given in FEMA 356 [7] under the stated earthquake levels. In the retrofitting design procedure of the buildings, the drift limits (roof displacement limit) used in the design of the buildings for each PL are obtained from NLSP analyses. These drift limits are determined based on the RC member rotation limits given in FEMA 356 [7] for each PL.

Most of the existing ordinary buildings (e.g. school, residential and low to mid-rise office buildings) have fundamental vibration periods that fall in the intermediate period range. In this period range, the energy dissipated by an elastic system can be assumed to be equal to an identical (nonlinear) system that yields at a certain lateral force level. The seismic retrofitting design methodology used in this study is mainly based on this equal energy dissipation principle. In the proposed methodology, the monotonic energy dissipation capacities of the buildings in the linear elastic range (based on the roof displacement obtained from RS analyses (Fig. 6(a))) and nonlinear inelastic cases (from NLSP analyses for each PL (Fig. 6(b))) were calculated and compared (Fig. 6(c)). The difference between the areas under the elastic and inelastic base shear force vs. roof displacement curves is the required additional energy that needs to be absorbed by the retrofitting system (e.g. PRS or SISP) (Fig. 6(d)). The step-by-step seismic retrofitting design procedure is given below. The design procedure needs to be repeated for each PL. The PL that yields a retrofitting design with the largest lateral strength governs the design.

1. In the first step, RS analyses of the building in the retrofitted stage are conducted to obtain the linear elastic base shear force vs. roof displacement relationship as shown in Fig. 6(a). Since the retrofitting scheme is not known at the initial stage

of the design procedure, the unretrofitted building is used in the analyses. However, since seismic retrofitting results in an increase in the lateral stiffness of the building, the lateral stiffness of the original building needs to be increased by a certain amount (e.g. initially by 20%) in the RS analyses by adjusting the modulus of elasticity of the RC members of the structure.

2. In the second step, the NLSP analyses of the original building are conducted to obtain the base shear force vs. roof displacement relationship. This relationship is plotted up to the displacement level corresponding to the displacement capacity of the building for the PL under consideration. The plotted curve is then idealized to have an elasto-plastic shape as described in FEMA 356 [5] (Fig. 6(b)). The yield base shear force, V_y, obtained from the elasto-plastic curve is used together with the elastic stiffness of the structure in the retrofitted stage (slope of the curve in Fig. 6(a)) to obtain a new elasto-plastic base shear force vs. roof displacement relationship (Fig. 6(c)) for subsequent calculations.
3. In the third step, first, the area, A_e, under the linear elastic base shear force vs. roof displacement curve is calculated. Then the area, A_p, under the elasto-plastic base shear force vs. roof displacement curve shown in Fig. 6(c) is calculated. The monotonic energy, A_d, that needs to be dissipated by the retrofitting system is then calculated as; $A_d = A_e - A_p$.
4. In this step, the required total strength, Q_1, of the retrofitting system at the base of the building is obtained with reference to Fig. 6(d) as follows.

$$Q_{1_{1,2}} = K_e d_p - V_y \mp \sqrt{(V_y - K_e d_p)^2 - 2K_e A_d} \tag{1}$$

One of the roots from the above equation will give the required strength, Q_1, of the retrofitting system at the base of the building.

5. In this step of the design procedure, first, the seismic shear force capacity, R_{Fi}, of each storey of the original unretrofitted building is obtained based on FEMA 356 [7] member rotation limits.
6. In this step of the design procedure, the retrofitting system is designed for the whole building. The design is based on uniform energy dissipation throughout the height of the building. For this purpose, the elastic shear, V_i, at each storey level, i is obtained from the RS analyses results in Step 1. Then, the total strength, R_1, at the base of the retrofitted building is obtained by summing up its base shear capacity, R_{F1}, and the required strength for retrofitting. That is; $R_1 = R_{F1} + Q_1$. To ensure uniform energy dissipation along the building height, the ratios of the total strength of the retrofitted building at each storey level i ($R_i = R_{Fi} + Q_i$) to the elastic shear, V_i, at the corresponding storey level must be equal. That is;

$$\frac{R_1}{V_1} = \frac{R_2}{V_z} = \cdots = \frac{R_i}{V_i} = \cdots = \frac{R_n}{V_n} \tag{2}$$

where the subscript, n, in the above equation denotes the number of stories. This will ensure that yielding is more likely to occur at all the storey levels. The ratio of the total strength, R_1, of the retrofitted building to the elastic shear V_1 at the base of the building is already known. To calculate the required retrofitting system strength at any storey level, i, the following relationship is used;

$$\frac{R_1}{V_1} = \frac{R_{Fi} + Q_i}{V_i}. \tag{3}$$

Then solving for Q_i, the following equation is obtained;

$$Q_i = \frac{R_1}{V_1} V_i - R_{Fi}. \tag{4}$$

7. The elastic stiffness of the designed building is recalculated and compared with the stiffness assumed in Step 1 of the procedure. If the difference is negligible the design is complete. Otherwise, the stiffness is updated and Steps 1, 3, 4, and 6 are repeated.

9.2. Sizing of the shear link and braces of the proposed retrofitting system

In this section, the procedure followed to determine the size of the link and braces of the PRS is presented. Following the procedure outlined above, the number of link-brace systems and the required link shear strength, Q_{Li}, at each storey level is already determined. The shear yield strength, V_y, of an HP, HE or W section is given as [35];

$$V_y = 0.6 F_y A_w \tag{5}$$

where F_y is the yield strength of steel, and A_w is the cross-section area of the web of the link. Setting $V_y = Q_{Li}$, the cross-section area, $A_{wi} = Q_{Li} / (0.6F_y)$ of the web at storey i is obtained. An HP, HE or a W section with the calculated web area, A_{wi}, is then chosen.

The ultimate failure mode for the shear link is inelastic web shear buckling. To ensure a stable energy dissipation mechanism throughout the cyclic loading history of the link in the PRS, this mode of failure may be delayed by adding stiffeners to the web of the link. The required stiffener spacing, a, for various shear link rotation demands, g_s, may be calculated using the following equation proposed by AISC [35] for shear links;

$$a = C_B t_w - 0.2d \tag{6}$$

where the constant $C_B = 56$, 38 and 29 respectively for g_s, $= 0.03$, 0.06 and 0.09 radians and d is the shear link depth.

Furthermore, the length, h_s, of the link needs to be determined such that yielding occurs in shear before its plastic moment capacity, M_p, is reached. Kasai and Popov [36] suggested that, due to the strain hardening effect, the shear link's plastic base moment, M_p, and shear, Q_{Li}, may increase. The increase in M_p and Q_{Li} is accompanied by large flange strains that may result in premature failure of the welded shear link–beam connection. To prevent such a failure, an upper bound of $1.2M_p$ and a corresponding shear of 1.5 Q_{Li} was suggested by Kasai and Popov [36]. Thus;

$$h_S < \frac{1.2M_p}{1.5Q_{Li}} = 0.8\frac{M_p}{Q_{Li}} \tag{7}$$

In the PRS, at the verge of buckling instability of the compression brace, the axial tensile and compressive forces in the tension and compression braces are both equal to the buckling load, P_b. Consequently, to prevent buckling instability of the compression brace, the sum of the horizontal components of the buckling loads of the two braces must be larger than the yield strength of the link times an over-strength factor, φ_s (Fig. 1(a)). Thus;

$$2P_b \cos\alpha \geq \phi_S Q_{Li}. \tag{8}$$

In the above equation, α is the angle that the braces make with the horizontal. Solving for P_b from the above equation, the required buckling strength of the brace is obtained as;

$$P_b = \frac{\phi_S Q_{Li}}{2cos\alpha}. \tag{9}$$

The braces are selected to have a minimum buckling capacity calculated from the above equation.

The details of the steel shear links and braces used for seismic retrofitting of the buildings and the details of the SISPs used in the conventional seismic retrofitting of the buildings are given in Table 4 for the x and y directions of the building respectively.

Table 4
Details of the steel and RC retrofitting members considered for nonlinear analyses.

School building							
PRS steel sections used in *x*-direction				SISP in *x*-direction	f_c' (MPa)	f_y (MPa)	Reinforcement (%)
Storey #	Link	Braces	Housing frame	Thickness (m)			
1	HE300M	HE200M	HE300M	0.15	20	420	0.40
2	HE260M	HE260M	HE260M	0.15	20	420	0.25
PRS steel sections used in *y*-direction				SISP in *y*-direction	f_c' (MPa)	f_y (MPa)	Reinforcement (%)
Storey #	Link	Braces	Housing frame	Thickness (m)			
1	HE260M	HE140M	HE260M	0.15	20	420	0.25
2	HE240M	HE120M	HE240M	0.15	20	420	0.25
Office building							
PRS steel sections used in *x*-direction				SISP in *x*-direction	f_c' (MPa)	f_y (MPa)	Reinforcement (%)
Storey #	Link	Braces	Housing frame	Thickness (m)			
2	HE200M	HE120M	HE220B	0.10 & 0.12	20	420	0.30 & 0.25
3	HE180M	HE100M	HE220B	0.10 & 0.12	20	420	0.21 & 0.20
4	HE180M	HE100M	HE220B	0.10 & 0.12	20	420	0.21 & 0.20
5	HE140M	HE100B	HE180B	0.10 & 0.12	20	420	0.13 & 0.13
6	HE140B	HE100B	HE180B	0.10 & 0.10	20	420	0.13 & 0.13
PRS steel sections used in *y*-direction				SISP in *y*-direction	f_c' (MPa)	f_y (MPa)	Reinforcement (%)
Storey #	Link	Braces	Housing frame	Thickness (m)			
1	HE200M	HE120M	HE220B	0.10	20	420	0.13
2	HE200M	HE120M	HE220B	0.10	20	420	0.13
3	HE200M	HE100M	HE220B	0.10	20	420	0.13
4	HE200M	HE100M	HE220B	0.10	20	420	0.13
5	HE160M	HE100B	HE180B	0.10	20	420	0.11
6	HE140B	HE100B	HE180B	0.10	20	420	0.11

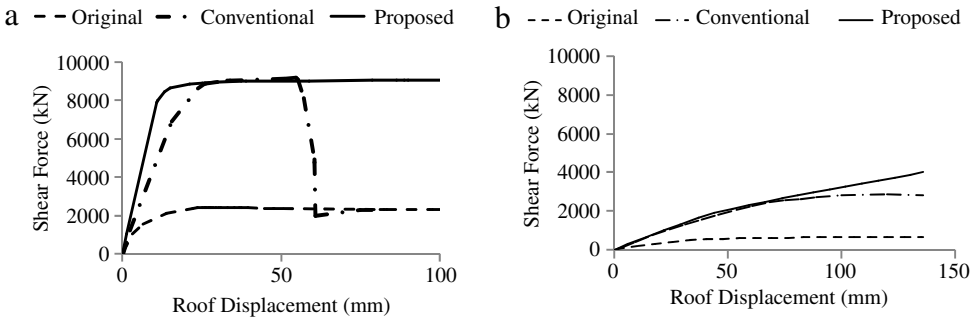

Fig. 7. (a) The base shear force as a function of the drift at the top-storey level for the school building in the *x*-direction. (b) The base shear force as a function of the drift at the top-storey level for the office building in the *x*-direction.

10. Nonlinear pushover analyses results

In this section, comparative performance evaluation of the original and seismically retrofitted buildings is performed using the NLSP analyses results.

The NLSP analyses results in the *x* direction of the school and office buildings for the original and retrofitted conditions are shown respectively in Fig. 7(a) and (b) in terms of base shear vs. roof displacement plots. The response in the *y*-direction is similar. From the figure, it is observed that the elastic lateral stiffness of the conventionally retrofitted structure using SISPs is smaller than the structure retrofitted with the PRS. This difference is attributed to the larger number of steel shear link–brace systems (PRS) required to achieve the same yield strength level as that of the SISPs. Thus, it is expected that the structure retrofitted with the PRS will have a smaller drift, and hence a more desirable performance (e.g. less non-structural damage) under the effect of small intensity earthquakes associated with the IO PL. Fig. 7(a) and (b) also demonstrate that the building retrofitted with the PRS produces a more stable lateral force–displacement relationship as compared to the building retrofitted with SISPs. The failure of the SISPs, which have limited drift capacities, causes loss of lateral strength of the conventionally retrofitted school building as observed from the figures. This clearly shows that the PRS have a larger monotonic energy dissipating and ductility capacity compared to that of the building retrofitted with SISPs and may potentially resist larger earthquakes. Compared to the original case, the buildings retrofitted with both PRS and SISPs exhibited a considerable increase in lateral stiffness and strength. This is indicative of a better seismic performance during a potential earthquake.

11. Nonlinear time history analyses results

Comparative performance evaluation of the original and retrofitted buildings is performed using the NLTH analyses results. The analyses results in terms of the maximum interstorey drift and roof displacement are presented for each earthquake as well as using the average of the analyses results from the seven earthquakes. Each earthquake is assigned a number (Table 3) to facilitate the presentation of the results.

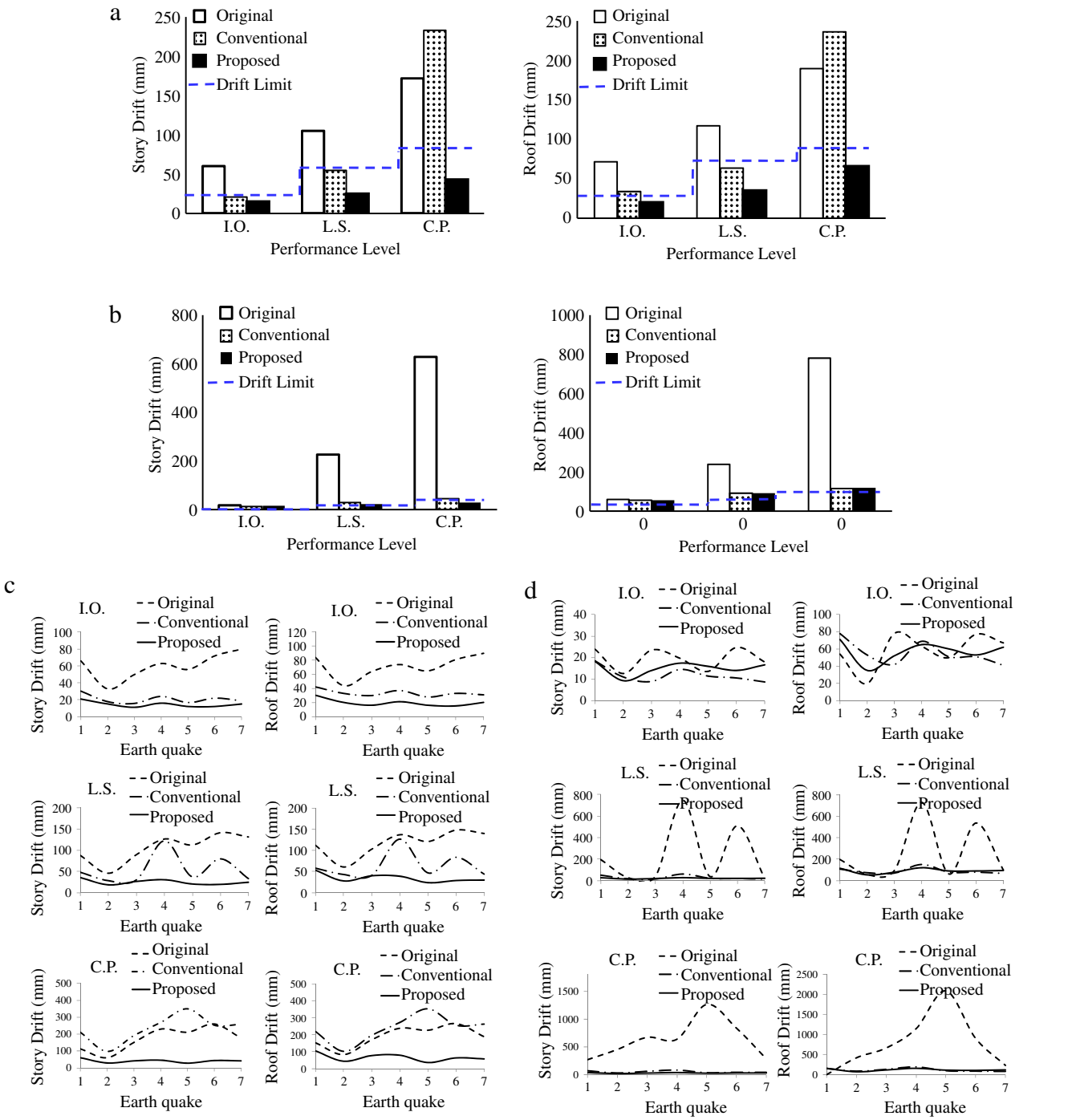

Fig. 8. (a) Average interstorey and roof drifts for the school building in the *x* direction. (b) Average interstorey and roof drifts for the office building in the *x* direction. (c) Maximum interstorey and roof drifts for the school building in the *x* direction. (d) Maximum interstorey and roof drifts for the office building in the *x* direction.

11.1. School building

Fig. 8(a) compares the average of the interstorey and roof drift demands in the *x*-direction from the seven earthquakes with the drift capacities respectively for the original building as well as the building retrofitted with the proposed (PRS) and conventional (SISPs) methods. The response in the *y*-direction is similar. As observed from the figure, for the unretrofitted building, the interstorey drift demands severely exceed the capacities (indicated by dashed lines and estimated based on the rotation limits of existing columns/beams) for all the PLs considered in the analyses. For the building retrofitted with the PRS however, the interstorey drift demands are smaller than the corresponding capacities for all the PLs considered in the retrofitting design. Nevertheless, this is not the case for the building retrofitted with SISPs. For this case, while the IO PL is completely satisfied, the interstorey drift demands at the LS and CP PLs for the first storey are larger than the corresponding capacities. It is worth noting that for the case of the building retrofitted with SISPs, the interstorey drift demands are even larger than those of the original building at the CP PL. The main reason for this type of behavior is the low ductility, heavy weight and considerable pinching in the hysteresis loops of the SISPs used in conventional retrofitting of the building. At the CP PL, the large intensity of the ground motions results in

large seismic forces acting on the structure. The added weight of the SISPs further amplifies the magnitude of these forces. Moreover, due to their low ductility, SISPs fail at small interstorey drift levels, rendering their stiffness and strength contribution ineffective during the earthquake. This sudden failure as well as larger structural weight due to the addition of SISPs results in amplified interstorey drift demands.

Fig. 8(c) displays the maximum interstorey drifts and maximum roof displacements of the original and seismically retrofitted buildings as a function of the earthquakes used in the analyses for each one of the seismic PLs (IO, LS, CP). Both seismic retrofitting techniques display a more desirable response than that of an unretrofitted building for the IO PL. However, for the LS and CP PLs, the response of the building retrofitted with SISPs becomes unsatisfactory as explained earlier. In addition, the building retrofitted with the PRS displays a highly stable response regardless of the characteristics (e.g. frequency content) of the earthquake used in the analyses (i.e. a more uniform or similar response is observed for all the earthquakes used in the analyses).

11.2. Office building

Fig. 8(b) compares the average of the interstorey and roof drift demands in the *x*-direction from the seven earthquakes with the drift capacities respectively for the original building as well as the building retrofitted with the proposed and conventional methods. The response in the *y*-direction is similar. Fig. 8(d) displays the maximum interstorey drifts and maximum roof displacements of the original and seismically retrofitted buildings as a function of the earthquakes used in the analyses for each one of the seismic PLs (IO, LS, CP) considered in the retrofitting design. The buildings retrofitted with both seismic retrofitting techniques display a more desirable response than that of an unretrofitted building for the IO PL. However, for the LS and CP PLs, the response of the building retrofitted with the conventional SISPs becomes unsatisfactory due to the extremely large drift demands due to the soft storey formation (as the SISPs fail), at the upper three storey levels of the office building.

12. Evaluation of the storey drifts along the buildings height

Maximum storey drift levels along the height of the buildings are shown to further assess the performance of the building retrofitted with the PRS in relation to those of the original building and the building retrofitted with conventional SISPs. The deformed shapes of the buildings are obtained at the instant when the maximum interstorey drift occurs.

12.1. School building

Fig. 9(a) compares the deformed shapes of the original building as well as the building retrofitted with the proposed and conventional methods for the average of the seven ground motions for IO, LS and CP PLs. The building retrofitted with the PRS has smaller interstorey drifts compared to those of the other buildings for all the seismic PLs considered. This is indicative of less damage in the case of a potential earthquake. Furthermore, compared to the original and the conventionally retrofitted building, the building retrofitted with the proposed technique exhibits a more uniform lateral deformation pattern, and hence a more even distribution of energy dissipation along the height of the building.

12.2. Office building

Fig. 9(b) compares the deformed shapes of the original building as well as the building retrofitted with the proposed and conventional methods for the average of the seven ground motions for IO, LS and CP PLs. For the IO PL, both the building retrofitted with the proposed and conventional method display similar deformed shapes. However, for the LS and CP PLs, the original building and the building retrofitted with the conventional SISPs display a less uniform distribution of interstorey drifts along the height of the building compared to that of the building retrofitted with the PRS. In the case of the original building a severe soft storey formation at the fifth-storey level is observed. The deformation of the building retrofitted with the conventional SISPs is mostly concentrated at the fifth- and sixth-storey levels (due to small column sizes) with the deformation at the lower storey levels being relatively modest. This resulted in slight soft-storey formations and the concentration of the energy dissipation at the fifth- and sixth-storey levels as observed from Fig. 9(a). Compared to the original and conventionally retrofitted building, the building retrofitted with the PRS exhibit smaller interstorey drifts, a more uniform lateral deformation pattern, and hence a more even distribution of energy dissipation along the height of the building.

13. Shear link rotations of the proposed retrofitting system

Kasai and Popov [10,36] conducted experimental tests on shear links made of stiffened W-sections. The test results indicated a maximum rotation capacity of 0.1 rad (the HE sections used in this study are stockier and hence may have larger rotation limits). The rotation values of the most critical shear links in the most critical PL (CP) are presented for *x* and *y* directions of the buildings in Fig. 9(c) and (d). For the school building while links 1–4 in Fig. 9(c) are located in the second storey, links 5–12 are located in the first storey. For the office building, links 1–5 in Fig. 9(d) are located in stories 6–2 respectively. As observed from the figures, all the link rotations are smaller than 0.1 rad. Thus, the shear links used as part of the PRS are expected to function as intended.

14. Damage analyses of the buildings

Damage analyses of the school and office buildings in the original and retrofitted conditions are performed to further assess the performance of the buildings retrofitted with the PRS in relation to those of the original building and the building retrofitted with the conventional SISPs. Seismic damage quantification is generally represented by damage indices that range between 0 (no damage) and 1 (complete collapse). The damage model proposed by Hindi and Sexsmith [37] is used in the damage analyses.

14.1. Damage model of Hindi and Sexsmith [37]

The damage model of Hindi and Sexsmith [37] is based on the monotonic energy dissipating capacity of structural elements before and after the application of reversed cyclic loading. The damage model takes as a reference the monotonic energy dissipation capacity of a structure in the undamaged virgin state, which is defined as the area, A_o, under the static pushover curve up to the point of failure. With the actual "n" cycles of load–displacement history applied on the structure due to a potential earthquake, the remaining monotonic energy dissipation capacity of the structure, compared to that in its virgin state, defines the extent of damage. The remaining monotonic energy dissipation capacity of the structure is defined as the area, A_n, under the static pushover curve obtained from the end of the last cycle, n, to the failure point. Accordingly, the damage index is defined as follows:

$$D_n = \frac{A_o - A_n}{A_o} \tag{10}$$

A damage index of 0 ($A_n = A_o$) is indicative of no damage, whereas a damage index of 1 ($A_n = 0$) is indicative of complete damage or collapse.

14.2. Damage analyses results

The results of the damage analyses of the school and office buildings for the *x* and *y* directions are presented in Fig. 10(a) and (b) respectively. In the figures, the averages of the damage indices

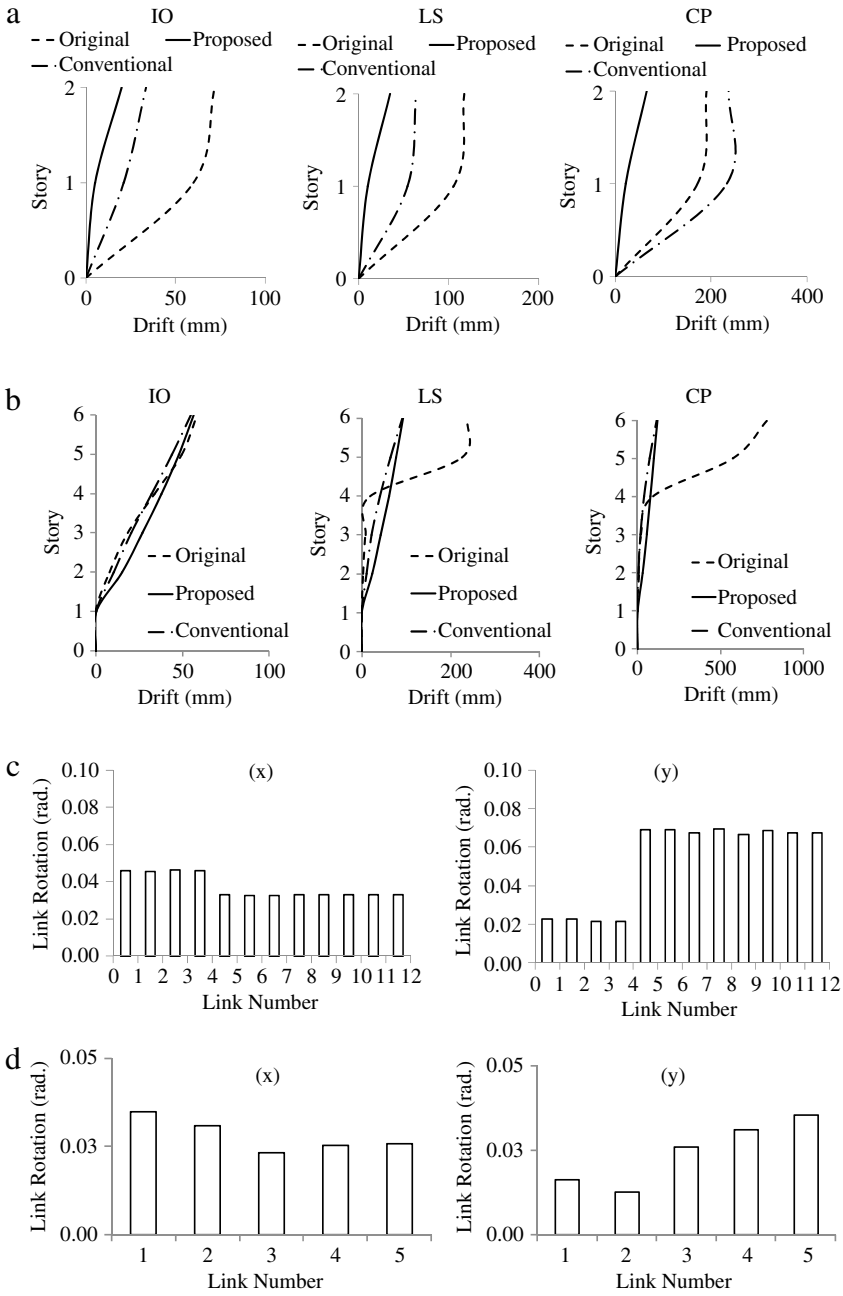

Fig. 9. (a) Maximum storey drifts along the height of the school building in the *x* direction. (b) Maximum storey drifts along the height of the office building in the *x* direction. (c) Shear link rotations for the PRS of the school building in the *x* and *y* directions. (d) Shear link rotations for the PRS of the office building in the *x* and *y* directions.

from the seven earthquakes used in the analyses are plotted as a function of the PL.

For the school building it is observed from Fig. 10(a) that for the IO PL a complete collapse ($D_n = 1$) of the original building is observed while the damage indices for the buildings retrofitted with the proposed (PRS) and conventional (SISPs) methods are quite low and comparable. For the LS and CP PLs the building retrofitted with the proposed method experiences significantly less damage than the one retrofitted with the conventional method.

For the office building. It is observed from Fig. 10(b) that for the IO PL severe damage ($D_n = 0.68$) to the original building is observed while the damage indices for the buildings retrofitted with the proposed and conventional methods are quite low and comparable. For the LS and CP PLs in the *y* direction, the building retrofitted with both methods have similar damage indices. However, in the *x* direction, the building retrofitted with the proposed method experiences significantly less damage than the one retrofitted with the conventional method. Thus, the damage analyses further reinforce the more desirable behavior of the building retrofitted with the proposed technique, as compared to that retrofitted with the conventional technique.

15. Conclusions

A seismic retrofitting system that combines the advantages of both conventional and modern retrofitting techniques is proposed. While the PRS can easily be designed and applied as in the case of conventional seismic retrofitting methods, it possesses a steel shear link that absorbs energy as in the case of RMTs (e.g. such as hysteretic dampers). Similar systems have also been proposed by other researchers where the link-brace system was directly applied as a simple retrofitting solution. However, in this research

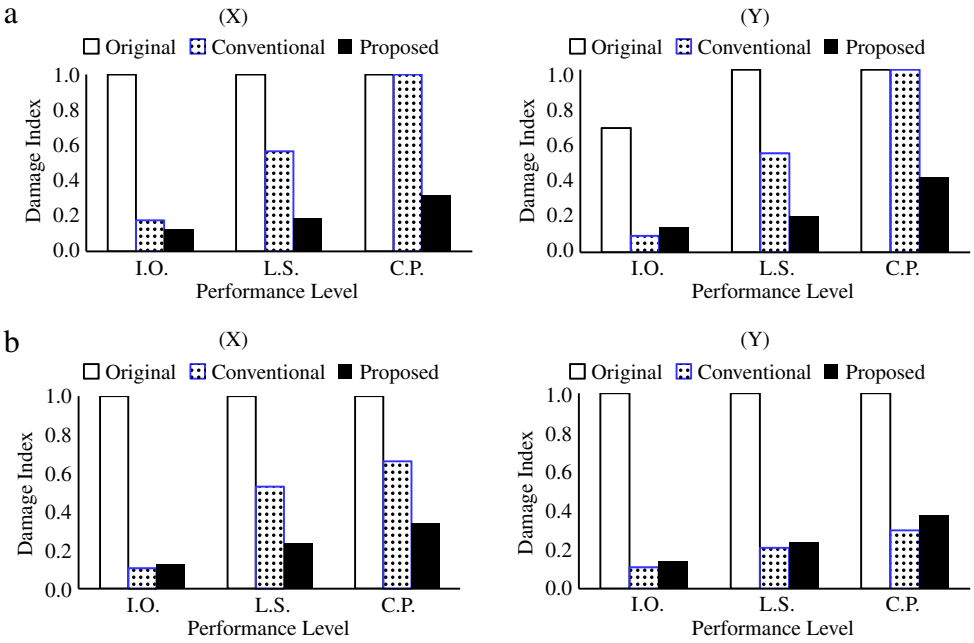

Fig. 10. Damage analyses results in the *x* and *y* directions: (a) school building, (b) office building.

study, the configuration of the proposed system in application to RC frames has been studied via 2-D and 3-D complex finite element analyses and a steel housing frame has been suggested for a more desirable structural performance. This study also offers a new performance based retrofitting design procedure that ensures a satisfactory performance of the retrofitted buildings using the PRS. In addition, this research presents a more realistic study based on actual buildings. Furthermore, in this research, the performance of the PRS is assessed in comparison to that of a conventional retrofitting system using SISPs to demonstrate the more desirable performance of the PRS compared to existing systems.

The efficiency of the PRS is tested via NLSP, NLTH and damage analyses of a school and an office building. The NLSP and NLTH analyses results revealed that the PRS can efficiently alleviate the detrimental effects of earthquakes on the buildings. The buildings retrofitted with the PRS have a more stable lateral force–deformation behavior with enhanced energy dissipation capability than that of the one retrofitted with SISPs. For IO PL (small intensity ground motions), the maximum inter-storey drift of the building retrofitted with the PRS is comparable to that of the one retrofitted with SISPs. But, for LS and CP PLs (moderate to high intensity ground motions), the maximum inter-storey drift of the building retrofitted with the PRS is considerably smaller than that of the one retrofitted with SISPs. Furthermore, compared with the building retrofitted with SISPs, for LS and CP PLs (medium to large intensity ground motions), the building retrofitted with the PRS experiences significantly less damage due to the more ductile behavior of the system.

References

[1] Endo T, Okifuji A, Sugano S, Ayashi T, Shimizu T, Takahara K. et al. Practices of seismic retrofit of existing concrete structures in Japan. In: Proc. of 8th world conference on earthquake engineering. vol. 1. 1984. p. 469–76.

[2] Ghobarah A, El-Attar M, Aly NM. Evaluation of retrofit strategies for reinforced concrete columns: a case study. Eng Struct 2000;22(5):490–501.

[3] Kelly JM. Aseismic Base isolation: review and bibliography. Soil Dynamics and Earthquake Engineering 1986;5(4):202–16.

[4] Tezcan SS, Erkal A. Seismic base isolation and energy absorbing devices. In: Yuksek Ogrenim ve Arastirma Vakfi Yayinlari. Istanbul: Higher Education and Research Foundation Publications; 2002.

[5] Soong TT, Spencer Jr BF. Supplemental energy dissipation: state-of-the-art and state-of-the-practice. Eng Struct 2002;24(3):243–59.

[6] Ahmad S, Ghani F, Adil R. Seismic friction base isolation performance using demolished waste in masonry housing. Constr Build Mater 2009;23(1):146–52.

[7] FEMA 356. Prestandard and commentary for the seismic rehabilitation of buildings. Washington (DC): Federal Emergency Management Agency. Building Seismic Safety Council; 2000.

[8] Dicleli M, Mehta A. Seismic retrofitting of chevron-braced steel frames based on preventing buckling instability of braces. Int J Struct Stab Dyn 2009;9(2):333–56.

[9] Bruneau M, Uang CM, Whittaker A. Ductile design of steel structures. New York, NY: McGraw Hill; 1998.

[10] Kasai K, Popov EP. General behavior of WF steel shear link beams. J Struct Eng 1986;112(2):362–82.

[11] Ghobarah A, Abou Elfath H. Rehabilitation of a reinforced concrete frame using eccentric steel bracing. Eng Struct 2001;23(7):745–55.

[12] Perera R, Gómez S, Alarcón E. Experimental and analytical study of masonry infill reinforced concrete frames retrofitted with steel braces. J Struct Eng 2004;130(12):2032–9.

[13] ANSYS. Structural simulation software. Canonsburg (PA, USA): SAS IP Inc.; 2009.

[14] Ministry of Public Works. Turkish seismic design code. Official Gazette. March 2007.

[15] Ministry of Public Works. Turkish seismic design code. Official Gazette. March 1975.

[16] IBC. International building code structural/seismic design manual — Volumes 1, 2, & 3. Sacramento (CA): Structural Engineers Association of California; 2000.

[17] DLH Seismic Design Guidelines. General Directorate for Construction of Railways, Harbors and Airports (RHA) of Ministry of Transportation: Republic of Turkey. 2006.

[18] SAP2000. Integrated finite element analysis and design of structures. Berkeley (CA, USA): Computers and Structures Inc.; 2006.

[19] Takeda T, Sözen MA, Nielsen NN. Reinforced concrete response to simulated earthquakes. J Struct Eng 1970;96(12):2557–73.

[20] Ilki A, Kumbasar N. Hysteresis model for reinforced concrete members. In: Proc. ASCE 14th engineering mechanics conference. Austin, on CD, University of Texas, Austin. 2000.

[21] Yalcin C, Saatcioglu M. Inelastic analysis of reinforced concrete columns. Comput & Structs 2000;77(5):539–55.

[22] Saatcioglu M, Humar JM. Dynamic analysis of buildings for earthquake-resistant design. Canad J Civil Eng 2003;30(2):338–59.

[23] Kwak HG, Kim DY. Material nonlinear analysis of RC shear walls subject to monotonic loadings. Eng Struct 2004;26(11):1517–33.

[24] Dowell RK, Seible F, Wilson EL. Pivot hysteresis model for reinforced concrete members. ACI Struct J 1998;95(5):607–17.

[25] Hsu TTC, Mo YL. Softening of concrete in torsional members — theory and tests. ACI Struct J 1985;82(3):290–303.

[26] Vecchio FJ, Collins MP. Compression response of cracked reinforced concrete. J Struct Eng 1993;119(12):3590–610.

[27] Mansour MY, Lee J-Y, Hindi R. Analytical prediction of the pinching mechanism of rc elements under cyclic shear using rotation-angle softened truss model. Eng Struct 2005;27(8):1138–50.
[28] Aoyama H, Kato D, Katsumata H, Hosokawa Y. Strength and behavior of postcast shear walls for strengthening of existing R/C buildings. In: Proc of eight world conference on earthquake engineering. vol. 1. 1984. p. 485–92.
[29] Kahn LF. Reinforced concrete infilled shear walls for aseismic strengthening. Ph.D. thesis. Ann Arbor (Michigan): University of Michigan; 1986.
[30] Hayashi T, Niwa H, Fukuhara M. Strengthening methods of the existing reinforced concrete buildings. In: Proceedings of the seventh world conference on earthquake engineering. vol. 4. 1980. p. 89–97.
[31] Sugano S. Aseismic strengthening of existing reinforced concrete buildings. In: Proc of the first seminar on repair and retrofit of structures. US/Japan Cooperative Earthquake Engineering Research Program. 1980.
[32] Higashi Y, Endo T, Ohkubo M, Shimizu Y. Experimental study on strengthening reinforced concrete structure by adding shear wall. In: Proc. of the seventh world conference on earthquake engineering. vol. 7. 1980. p. 173–80.
[33] Smith B, Coull A. Tall building structures analysis and design. New York: Wiley; 1991.
[34] Acun B, Sucuoğlu H. Comparative evaluation of the performance limit states of reinforced concrete columns in view of experimental observations. 2010 (in press).
[35] Specification for Structural Steel Buildings. Chicago (IL): AISC, American Institute of Steel Construction; 2005.
[36] Kasai K, Popov EP. Cyclic web buckling control for shear link beams. J Struct Eng 1986;112(2):362–82.
[37] Hindi RA, Sexsmith RG. A proposed damage model for RC bridge columns under cyclic loading. Earthquake Spectra 2001;17(2):261–90.